

Nonlinear effects in a liquid crystal optical oscillator

S. Residori^{*a}, U. Bortolozzo^{*b}, Jean-Pierre Huignard^c, A. Montina^d, F.T. Arecchi^d

^aINLN, Université de Nice Sophia-Antipolis, CNRS, 1361 route des Lucioles, 06560 Valbonne, France

^bLaboratoire de Physique Statistique de l'ENS, 24 me Lhomond, 75231 Paris Cedex 5, France

^cThales Research & Technology, RD 128 91767 Palaiseau Cedex, France

^dPhysics Department, University of Florence, Largo E. Fermi 6, 50125 Florence, Italy

ABSTRACT

A nonlinear optical medium results by the collective orientation of liquid crystal molecules tightly coupled to a transparent photoconductive layer made of a BSO photorefractive crystal. The nonlinear medium, called photorefractive liquid crystal light-valve, gives a large two-wave-mixing gain, thus, when inserted in a ring cavity, it results in an unidirectional optical oscillator. Dynamical regimes with many interacting modes are made possible by the wide transverse size and the high nonlinearity of the liquid crystal gain medium. In particular, we show the generation of spatiotemporal pulses, coming from the random superposition of many longitudinal and transverse modes simultaneously oscillating in the cavity.

Keywords: Liquid crystals, Nonlinear optics, Two-wave mixing, Spatiotemporal pulses

1. INTRODUCTION

A laser is a positive feedback optical amplifier. The active medium with population inversion acts as the light amplifier by means of stimulated emission and the cavity supplies the feedback [1]. The two-wave mixing in photorefractive crystals provides another mechanism of light amplification [2] and has been intensively used in the past to observe a rich variety of spatiotemporal dynamics of the transverse cavity modes [3]. Because of the limited transverse size of photorefractive crystals, the number of activated modes is relatively small, typically about few tens. Recently, we have introduced a new optical oscillator based on a liquid crystal light valve (LCLV) as a gain medium [4]. The large transverse size and high gain of the LCLV allows a large number of longitudinal and transverse modes to be simultaneously amplified in the cavity, thus giving rise to dynamical regimes remained inaccessible up to date.

We report different dynamical regimes, in particular high amplitude spatiotemporal pulses that appear in random space points and are confined along the three space directions. Even though several theoretical predictions have been given in the past [5-7], our observations are the first experimental evidence of 3D confined optical structures. The mechanism for the formation of spatiotemporal pulses has to be searched in local interference effects between the huge number of modes that are traveling in the cavity at different angles and with different frequencies. A similar mechanism has been recently employed to synthesize spatiotemporal pulses in a linear optical system [8]. However, in our experiment the superposing fields are not created by externally imposed gratings but are instead spontaneously generated in the cavity through nonlinear interactions in the LCLV.

Together with the experimental observations, we present also a theoretical model that takes into account the longitudinal dependence of the cavity field, thus allowing for the formation of 3D optical structures. The model is derived starting from the Maxwell equations for the light propagation in the cavity and from the theory of the LCLV. The main differences with respect to existing models of cavity oscillators [9-10] are due to the specific features of the gain medium. Indeed, the large number of transverse and longitudinal modes prevents the use of a mean field approximation along the cavity axis and needs for considering the longitudinal variations of the cavity field. For a set of parameters consistent with the experiment, we perform numerical simulations confirming the appearance of 3D localized spatiotemporal pulses.

*stefania.residori@inln.cnrs.fr; phone +33 4 92967317; fax +33 4 93652517

Liquid Crystals XI, edited by Iam Choon Khoo, Proc. of SPIE Vol. 6654, 665406, (2007) . 0277-786X/07/\$18 . doi: 10.1117/112.730358

2. THE LIQUID CRYSTAL LIGHT-VALVE AS A LIGHT AMPLIFIER

The photorefractive liquid crystal light-valve combines a liquid crystal layer with a thin monocrystalline $\text{Bi}_{12}\text{SiO}_{20}$ (BSO) photorefractive crystal. In this device, both photoconductive and electro optic properties are separately optimized. While the excellent photosensitivity arises from the photoconductive properties of the BSO, the large electro-optic effect is due to the large birefringence of the liquid crystals [11]. The LCLV is schematically represented in Fig.1a. It is realized by using a BSO crystal as one of the walls. The BSO is cut in the form of a thin slice, $d=1$ mm thickness, 20×30 mm lateral sizes. On one side it is coated with an Indium-Tin-Oxide (ITO) transparent electrode. The other wall of the cell is a glass window (BK7) coated with ITO. Both the BSO surface and the ITO side of the glass window are treated with polyvinyl-alcohol (PVA), polymerized and then rubbed to obtain planar alignment of the liquid crystals. Teflon spacers of $14 \mu\text{m}$ are inserted between the two walls and the cell is sealed with UV photo-polymerizing glue.

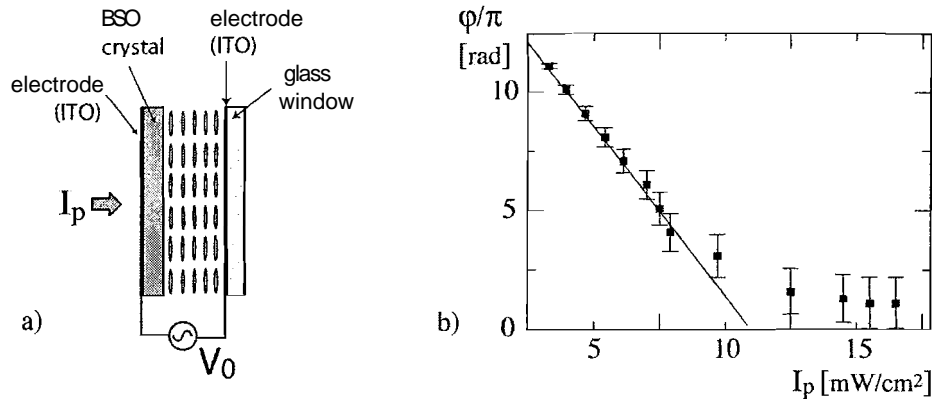


Fig. 1. a) Schematic representation of the photorefractive liquid crystal light-valve. b) Typical response of the LCLV as a function of the pump beam intensity I_p ; the applied voltage is fixed to $V_0 = 20$ V *rms*, frequency $f = 20$ KHz.

The assembled cell is filled with the nematic liquid crystal E48 that has a positive dielectric anisotropy, $\Delta\epsilon = 15.1$ at 1.0 kHz, and optical birefringence $\Delta n = n_e - n_o = 0.2306$, the extraordinary and the ordinary index being, respectively, $n_e = 1.7536$ and $n_o = 1.5230$ at $\lambda = 589.3$ nm and $T = 20$ °C. The final quality of the planar alignment is tested under a polarizing microscope.

The BSO crystal, well-known for its photorefractive properties [12], is here used for its large photoconductivity in the visible range, from $\lambda = 400$ to 550 nm. An AC voltage V_0 is applied across the cell through the ITO electrodes. Under the application of an electric field, liquid crystals tend to realign in such a way to become parallel to the direction of the applied field. When the light intensity on the BSO increases, its impedance decreases due to the photoconductivity and hence, the voltage drop across the liquid crystal layer increases, inducing liquid crystal reorientation. As a consequence, a light beam passing through the liquid crystal layer experiences a refractive index change and, thus, a phase change ϕ . A typical response of the LCLV is displayed in Fig.1b. It was obtained by inserting the LCLV between two crossed polarizers, with the liquid crystal director making an angle of 45° with their axes, and by sending on the photoconductor side a pump, $\lambda = 532$ nm, and a probe beam, $\lambda_0 = 632$ nm [13]. The phase change experienced by the probe beam is $\phi = 2\pi \Delta n l / \lambda_0$ with $l = 14 \mu\text{m}$ the thickness of the liquid crystal layer and $\Delta n = n(\theta) - n_o$ the refractive index change, θ being the liquid crystal tilt angle.

The measured phase change ϕ is plotted in Fig.1b as function of the pump intensity I_p . The saturation of the response is attained when the liquid crystal molecules are aligned along the direction of the applied field. The full range of phase variation is $\phi \approx 11\pi$, which corresponds to the maximum birefringence $\Delta n = n_e - n_o \approx 0.2$ for the initial planar alignment of the liquid crystals. In the linear part of the response the LCLV behaves as a Kerr-like nonlinear medium, with a refractive index change $\Delta n \propto I_p$, proportional to the intensity I_p of the light illuminating the BSO side.

For an incident illumination of 1 mW/cm^2 in the green, $\lambda = 532$ nm, the typical response time of the LCLV is of the order of 100 ms. The spatial resolution has been determined by measuring the contrast of the hexagonal patterns arising in a

feedback inirror configuration [13] and it has been found to be about $N=30$ lp/mm, which corresponds to a lateral diffusion length $l_D=20$ μ m.

2.1 Two-wave mixing gain and signal amplification

To determine the nonlinear coefficient of the LCLV and its amplification gain, we have performed two-wave mixing (2WM) experiments. The experimental setup is shown in Fig.2a. A weak signal beam, $I_s(0)$, is sent to the LCLV together with a high intensity pump beam, $I_p(0)$. The ratio between the pump and signal intensities is fixed to $\beta=80$. The two beams interfere in the plane of the BSO, giving rise to a fringe pattern, hence to local reorientation of the liquid crystal molecules in correspondence to the local increase of the voltage drop. Thus, the molecular reorientation follows the intensity fringe pattern and a refractive index grating is formed inside the liquid crystal layer.

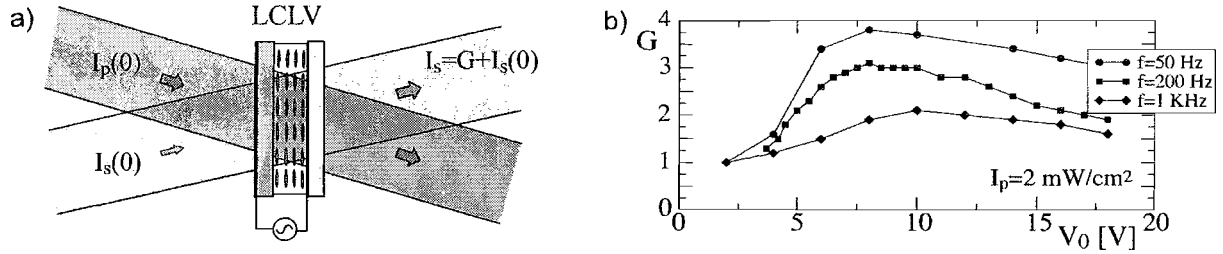


Fig. 2. Two wave mixing experiment: a) experimental setup. b) Gain G measured as a function of the applied voltage V_0 .

The two writing beams are self-diffracted by the refractive index grating that they have induced inside the cell. Since the liquid crystal layer is thin, the self-diffraction of the two beams is in the Raman-Nath regime [14]. Under this condition, the diffraction efficiency is given by

$$\eta = J_1^2\left(\frac{\pi\Delta n l}{\lambda}\right) \approx \left(\frac{\pi\Delta n l}{\lambda}\right)^2, \quad (1)$$

where J_1 is the Bessel function of the first order, $\Delta n = n(\theta) - n_0$ is the refractive index change due to the reorientation of the liquid crystal molecules and l is the thickness of the liquid crystal layer. If the pump beam is much more intense than the signal beam, $I_p(0) \gg I_s(0)$, then at the signal beam at the exit of the cell can be expressed as

$$I_s(l) = I_s(0) + \eta I_p(l), \quad (2)$$

and if we define the two-wave-mixing gain as $G = I_s(l)/I_s(0)$, we obtain

$$G = 1 + \left(\frac{2\pi n_2 I_p}{\lambda}\right)^2 l^2, \quad (3)$$

where $\mathbf{An} = 2n_2\sqrt{I_p I_s}$ is the amplitude of the refractive index grating, with $n_2 = \frac{\partial n(I)}{\partial I}$ the nonlinear optical coefficient of the LCLV.

In the LCLV the beam coupling always takes place in such a way that the energy transfer is towards the beam with lower intensity. The measured gain is plotted in Fig.2b as a function of the applied voltage V_0 and for different frequencies of the voltage. The maximum value obtained for $\beta=80$ and $I_p=1.8$ mw/cm^2 is $G \approx 4$, which corresponds to $n_2 = 5.4$ cm^2/W . Note that the LCLV works in the Raman-Nath regime, so that, even though the nonlinear coefficient is very high, the overall gain is limited, since for high pump intensity there are several diffraction orders into which the energy is redistributed. For thicker cells, that is, by approaching the Bragg diffraction regime, we should be able to obtain larger values of G . Another way to increase the gain is that of using several cells in cascade, as demonstrated in Ref.[15].

3.1 Spatiotemporal pulses

For a fixed and large Fresnel number, $F=500$, and by changing V_0 and the pump intensity I_p , we have determined the experimental phase diagram, as reported in Fig.4. Cavity mode oscillations are in the larger grey area whereas spatiotemporal pulses are in the darker area. The low V_0 regimes are similar to those observed for low F , with the alternation of low order Gauss-Laguerre modes. The transition to the high V_0 regimes is accompanied by the emission of high order and out of axis symmetrical modes. For intermediate values of V_0 and I_p , a large number of modes interact through the nonlinear medium occupying the whole size of the area illuminated by the pump and giving rise to spatiotemporal pulses. These appear as large intensity peaks over a lower amplitude and "speckle-like" background.

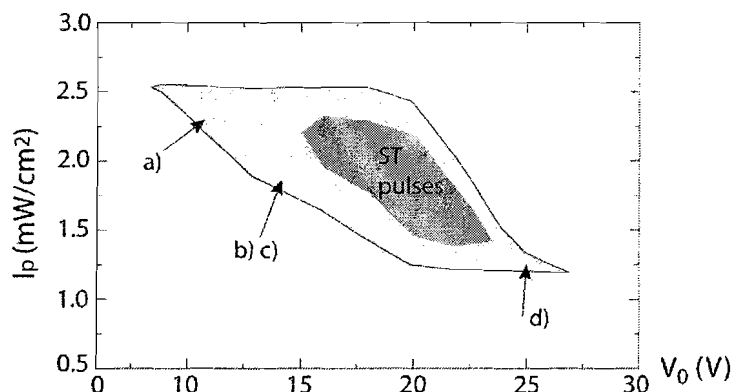


Fig. 4. Experimental phase diagram in the V_0 versus I_p space.

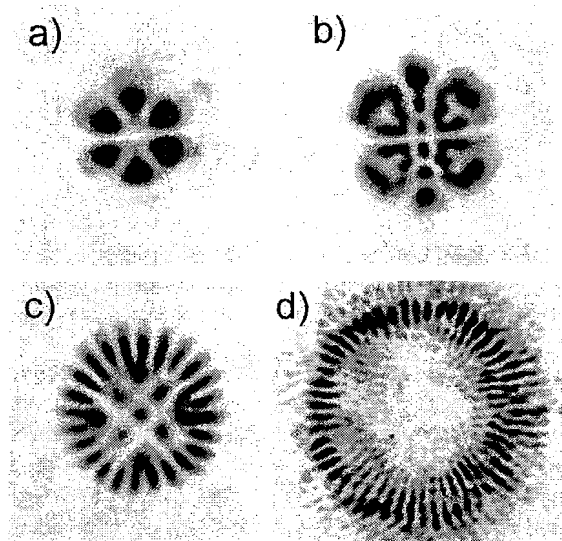


Fig. 5. Instantaneous snapshots showing the transverse intensity distribution for different dynamical regimes; a) alternation of low order Gaussian modes, $V_0=10$ V, $I_p=2.4$ mW/cm²; b) and c) higher order modes alternating during the time for $V_0=14$ V, $I_p=2.0$ mW/cm²; d) large ring modes observed for $V_0=25$ V, $I_p=1.3$ mW/cm².

Instantaneous snapshots of the transverse intensity distributions $I_c(x,y)$ are displayed in Fig5. The transverse size of the oscillating field increases with V_0 , up to a large ring for high V_0 . The spatiotemporal pulses appear when a large number of modes is populating the whole size of the area illuminated by the pump beam. A typical snapshot corresponding to this case is displayed in Fig.6a and the corresponding spatiotemporal plot is shown in Fig.6b.

To investigate the dynamical features of spatiotemporal pulses we have fixed $V_0=20.3$ V *rms* and $I_p=2.0$ mW/cm² and we have recorded several movies. The spatiotemporal pulses are identified by applying on each frame a threshold of 3 times

the average intensity $\langle I_c \rangle$ calculated over the entire set of frames in any experimental run. The extension of the pulses in the z direction is investigated by simultaneously recording the intensity distributions at the three planes z_1 , z_2 and z_3 plane. The three CCD are driven by the same trigger, whose delay time is negligible with respect to the liquid crystal response time. We select $z_1=0$, $z_2=5$ and $z_3=32$ cm. The magnification ratio, the size of the window and the intensity levels are the same for the three planes. Three spatial profiles recorded at the three different planes are displayed in Fig.7. By reslicing the movie recorded in z_2 along the direction joining the two pulses and by keeping the temporal dependence, we obtain the spatiotemporal profile shown in Fig.8.

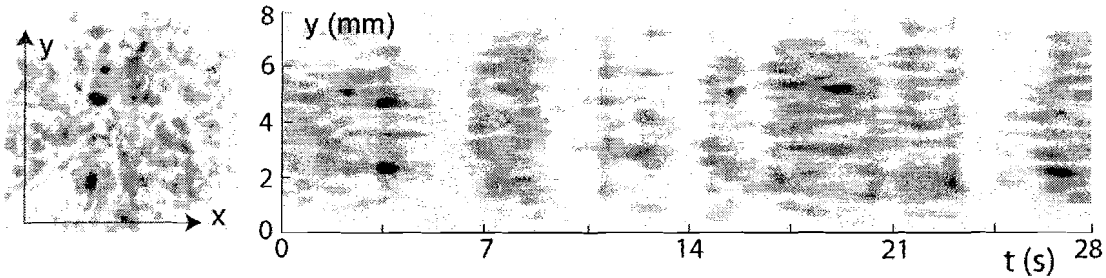


Fig. 6. Spatiotemporal pulses observed for $V_0=20$ V, $I_p=2.0$ mW/cm²; a) instantaneous snapshot; b) spatiotemporal plot obtained by cutting the movie along the y direction.

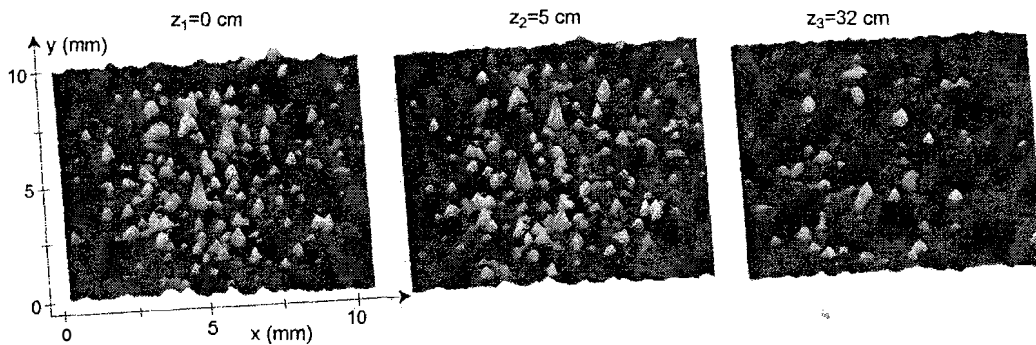


Fig. 7. Spatial profiles recorded at z_1 , z_2 and z_3 . Colors on line, from blue (minimal intensity) to red (maximal intensity).

It can be seen from Fig.7 that at z_3 the two large pulses have disappeared whereas from Fig.8 we see that the pulses have a limited temporal extension. By taking the half height width of the pulses with $I_c(x,y,z) > 3 \langle I_c \rangle$ and by averaging over more than one hundred profiles, we find that the transverse size of a pulse is 250 ± 50 μm whereas its average lifetime is around 0.5 ± 0.1 s. As for the longitudinal extension, by inspecting several movies taken at different z_3 , we estimate it around 30 cm.

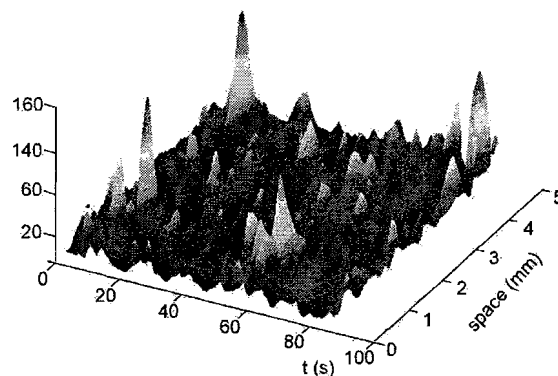


Fig. 8. Spatiotemporal profile extracted from the z_2 movie.

4. THEORETICAL MODEL

The model for the liquid crystal oscillator is derived by coupling the Maxwell equations for the cavity field with a Debye relaxation equation for the refractive index change in the liquid crystal layer [16]. The model takes into account the Kerr nonlinearity of the medium as well as the 2WM mechanism of photon injection inside the cavity. The LCLV is positioned in $z=0$, perpendicularly to the cavity axis and (x,y) denotes the coordinates in the transverse x,y plane. The refractive index $n(x,y,t)$ satisfies the equation

$$\tau \frac{\partial n(x,y,t)}{\partial t} = n_c - n + l_D^2 \nabla_{\perp}^2 n + \alpha |E(x,y,t)|^2, \quad (4)$$

where ∇_{\perp}^2 is the transverse Laplacian, l_D the transverse diffusion length and α the nonlinear coefficient of the LCLV, n_c a constant value determined by the voltage V_0 applied to the LCLV. The total electric field at the entrance of the liquid crystal layer is

$$E(x,y,t) = E_p e^{i(k_p \cdot r - \omega_p t)} + E_c e^{i(k_c \cdot z - \omega_p t)} + c.c., \quad (5)$$

where $E_c = E_c(x,y,t)$ is the complex amplitude of the cavity field and E_p is the amplitude of the pump plane wave, which is taken as constant. The intensity at the entrance side of the LCLV is

$$|E|^2 = |E_p|^2 + |E_c|^2 + \frac{1}{2} E_p^* E_c e^{-ik_{\perp} \cdot r_{\perp}} + c.c. \quad (6)$$

and gives rise to a refractive index change with two components, one varying slowly in space, the other corresponding to a spatial grating with wave number $k_{\perp} = k_p - k_c$. We thus write the refractive index as

$$n(x,y,t) = n_c - \alpha |E_p|^2 + n_0 + n_1 e^{-ik_{\perp} \cdot r_{\perp}} + c.c., \quad (7)$$

where $|E_p|^2$ is constant. When we substitute this expression in the equation for n we obtain

$$\tau \frac{\partial n_0}{\partial t} = (-1 + l_D^2 \nabla_{\perp}^2) n_0 + \alpha |E_c|^2, \quad (8)$$

$$\tau \frac{\partial n_1}{\partial t} = \left(-1 - 2il_D^2 k_{\perp} \cdot \nabla + l_D^2 \nabla_{\perp}^2 - l_D^2 |k_{\perp}|^2 \right) n_1 + \alpha E_p^* E_c, \quad (9)$$

for the slowly varying fields n_0 and n_1 .

The wave equation for the cavity field is written for a planar cavity by adopting the slowly varying amplitude approximation and by considering n_0 and n_1 small. Due to the large scale separation between the medium response time and the cavity round-trip time, we neglect the time derivative and get

$$\frac{\partial E_c}{\partial z} = \left(\frac{i}{2k} \nabla_{\perp}^2 + ikn_0 W(z) + \frac{i\delta - \gamma_c}{c} \right) E_c + ikn_1 W(z) E_p(z), \quad (10)$$

where $W(z)=1$ in the liquid crystal layer and 0 elsewhere, δ is the phase shift acquired by the cavity field in a round trip, γ_c is the cavity loss rate, $E_p(0)=E_p$ and we have assumed $k \approx k_p \approx k_c$.

Since the liquid crystal layer is thin, inside the medium we neglect the transverse Laplacian and we consider the 2WM in the Raman-Nath diffraction regime. Thus, inside the medium we have to take into account multiple order scatterings of the pump [16]. By doing this, we obtain the following expression for the cavity at the exit of the LCLV

$$E_c(l) = e^{ik l n_0} \left(J_0(2kl|n_1|) E_c + i \frac{n_1}{|n_1|} J_1(2kl|n_1|) E_p(0) \right), \quad (11)$$

where J_0 and J_1 are the Bessel functions of order zero and one, respectively.

Outside the LCLV the field evolution is governed by diffraction, thus the transverse Laplacian has to be retained. By considering that the cavity field has to satisfy the periodic boundary conditions imposed by the cavity, including the presence of the lens, it can be shown that the cavity field at the entrance of the LCLV is given by

$$E_c(x, y) = i \sum_{s=0}^{\infty} D^s G E_p(0) \quad (12)$$

where

$$D = C e^{i k n_0} J_0(2k|n_1|) \quad (13)$$

is the operator describing the mutual coupling between the cavity modes

$$G = C e^{i k n_0} \frac{n_1}{|n_1|} J_1(2k|n_1|) \quad (14)$$

is the operator accounting for the 2WM process of photon injection inside the cavity and

$$C = \Gamma^{1/2} e^{i\delta} S^m e^{i(L-L_1/2k)\nabla_{\perp}^2} e^{-i(k/2f)r_{\perp}^2} e^{i(L_1/2k)\nabla_{\perp}^2} \quad (15)$$

is the operator describing the field propagation inside the cavity. L_1 is the distance between the LCLV and the lens, $(1-\Gamma)$ is the fraction of lost photons in a round trip, δ is the phase shift acquired by the cavity field in a round trip and S is the specular operator, m being the number of mirrors of the cavity (S exchanges \mathbf{r}_{\perp} with $-\mathbf{r}_{\perp}$).

Equations (8,9) and equation (12) constitute our model. The first two equations describe the dynamics of n_0 and n_1 and contain the cavity field E_c , given by the last equation as a function of the refractive indices. Eq.(12) has a simple physical interpretation. The first term with $s=0$ gives the field scattered by the LCLV into the cavity with $E_c=0$ and its subsequent evolution in a round trip. The other terms are the contribution of this field after s returns to the LCLV. Because of the cavity losses, this series converges and can be approximated by a finite number of terms.

4.1 Analysis of the model in the one-mode approximation

In the linear regime the cavity field grows exponentially above a threshold value of the pump intensity, until saturation terms become relevant. We assume that only one longitudinal, one transverse mode of the cavity is nearly resonant and undergoes oscillations. This condition can be experimentally obtained by putting a diaphragm inside the cavity and by closing it in such a way that only the fundamental transverse mode is selected. The selection of the longitudinal mode takes place through the frequency detuning with respect to the pump field, as it follows from the analysis below. In the one mode approximation the operator equation to obtain the cavity field is replaced by the scalar one

$$E_c(0) = i \frac{n_1}{|n_1|} \frac{\Gamma^{1/2} e^{i(\delta_0 + k \ln_0)} J_1(2k|n_1|)}{1 - \Gamma^{1/2} e^{i(\delta_0 + k \ln_0)} J_0(2k|n_1|)} E_p(0), \quad (16)$$

where δ_0 is the phase acquired by the cavity field in a round trip, i.e.,

$$\frac{\delta_0 c}{L} \equiv \omega_0, \quad (17)$$

is the frequency detuning of the cavity mode with respect to the pump field. Let us assume that the eigenmode is smooth with respect to the diffusion length l_D , then Eqs.(8,9) become, respectively,

$$\tau \frac{dn_0}{dt} = -n_0 + \alpha |E_c|^2, \quad (18)$$

$$\tau \frac{dn_1}{dt} = \left(-1 - I_D^2 |k_{\perp}|^2 \right) n_1 + \alpha E_p^* E_c. \quad (19)$$

We now linearize Eqs.(18,19), in order to study the stability of the stationary solution $n_0=n_1=0$ and find the threshold condition for the cavity oscillation. The first equation gives $\tau dn_0/dt = -n_0$, thus we can take $n_0=0$ and consider only the second equation, which yields

$$\tau \frac{dn_1}{dt} = \left(-1 - I_D^2 |k_{\perp}|^2 + \alpha I_p \frac{i\Gamma^{1/2} e^{i\delta_0}}{1 - \Gamma^{1/2} e^{i\delta_0}} \right) n_1 \equiv c_2 n_1. \quad (20)$$

The threshold condition is $\text{Re}[c_2] > 0$, i.e.,

$$-1 - I_D^2 |k_{\perp}|^2 - \alpha I_p \frac{\sin \delta_0}{1 + \Gamma - 2\Gamma^{1/2} \cos \delta_0} > 0. \quad (21)$$

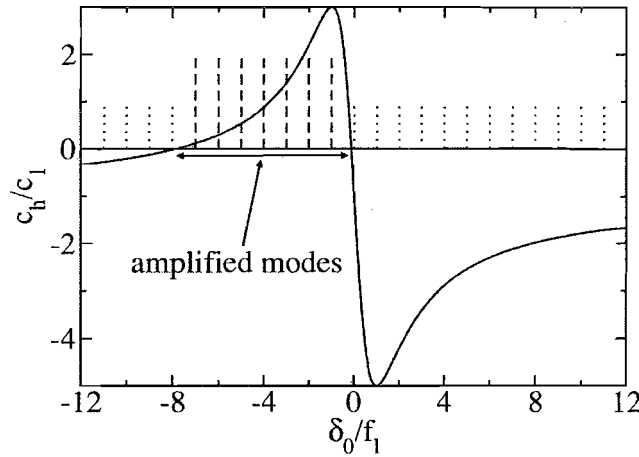


Fig. 9. c_h/c_1 as a function of δ_0/γ for $\alpha I_p/\gamma c_1=8$. The dashed lines represent the amplified modes of the cavity. The dot lines are the sub-threshold ones.

The second term is zero at $\delta_0=0$ and has a maximum at $\delta_0=\delta_0^M$ for which the threshold value of αI_p is minimal and given by

$$|\alpha I_p^{\text{thr}} = \frac{1-\Gamma}{\Gamma^{1/2}} \left(1 + I_D^2 |k_{\perp}|^2 \right) \quad (22)$$

For cavities with very small losses, the threshold condition becomes

$$\frac{c_h}{1 + I_D^2 |k_{\perp}|^2} \equiv -1 - \frac{\alpha I_p}{1 + I_D^2 |k_{\perp}|^2} \frac{\delta_0}{\gamma^2 + \delta_0^2}, \quad (23)$$

where $\gamma \equiv 1 - \Gamma^{1/2} \ll 1$. In Fig.9 we report c_h/c_1 as a function of δ_0/γ for $\alpha I_p/\gamma c_1=8$. The dashed lines represent the resonant modes and have a negative δ_0 , whereas the dot lines are the sub-threshold modes. For high negative detuning the gain decreases and becomes negative, because of the phase mismatch among the cavity fields with different number of round trips (in other words, the terms in the series of Eq.(11) sum up to zero because of destructive interference effects).

It is interesting to note that the imaginary part of c_2 gives a phase rotation of n_1 and, consequently, of E_c . Thus, the cavity field has a phase drift with respect to the pump E_p . The corresponding frequency difference, called pulling [1], is always negative and for $\gamma \ll 1$ equal to

$$\omega_{\text{pull}} = -\frac{1}{\tau} \frac{\alpha I_p \gamma}{\gamma^2 + \delta_0^2}. \quad (24)$$

At the threshold and for $\delta_0 = \delta_0^M$

$$\left| \omega_{\text{pull}}^{\text{thr}} \right| \approx \frac{c_1}{2\tau}, \quad (25)$$

i.e., it is of the order of the relaxation rate of n_1 .

4.2 Two-dimensional numerical simulations

We have performed numerical simulations of the model equations, Eqs.(8,9) and Eq.(12), for one transverse dimension x . The parameters are chosen from the experiment, $\tau=40$ ms, $l_D=30$ μm , $I_p=2$ mW/cm^2 and $a=4$ cm^2/W and set to a regime where many modes are present. The number of terms in the sum is truncated to the number of round-trips given by the average lifetime of photons in the cavity. In Fig.10a we show the intensity distribution calculated in the x,z plane at a fixed time, whereas in Fig.10b is shown a spatiotemporal profile at a fixed z . As in the experiment, spatiotemporal pulses appear as light filaments confined both in the transverse and longitudinal direction.

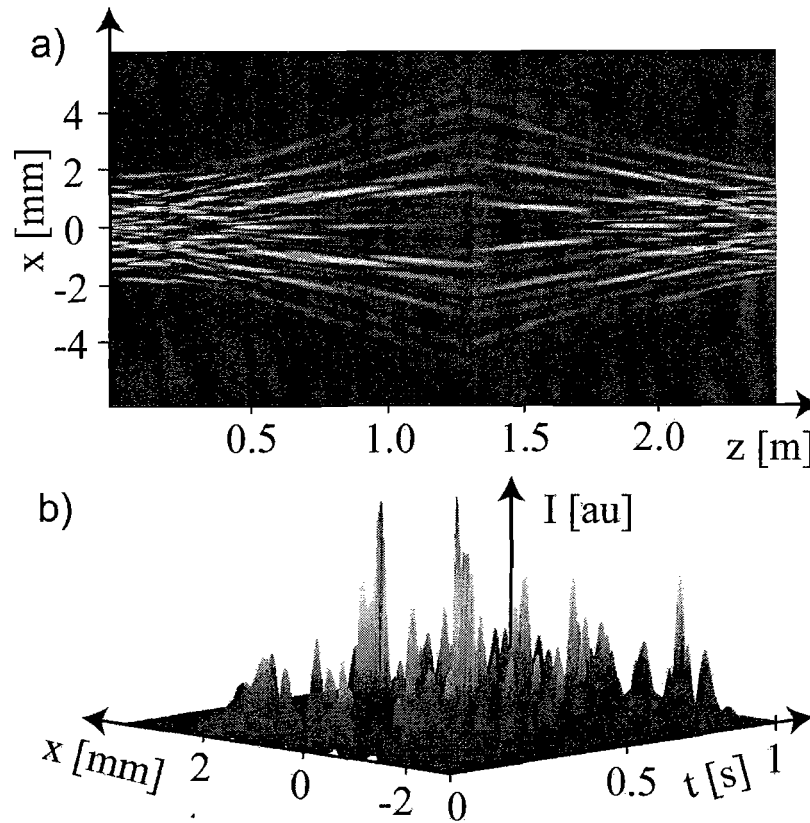


Fig. 10. Numerically calculated field distributions: a) a cut in the $x-z$ plane at a fixed time; b) a spatiotemporal profile at a fixed z . The dashed line in a) marks the lens position ($L_1=1.3$ m, $L_2=1.1$ m and $f=0.7$ m). Colors on line.

5. CONCLUSIONS

In conclusion, we have shown that a novel type of nonlinear optical oscillator can be built by using a liquid crystal light-valve as the gain medium. We have reported different dynamical regimes and we have given evidence of 3D confined spatiotemporal pulses. We have developed a theoretical model that takes into account the Kerr nonlinearity of the medium as well as the two-wave-mixing mechanism of photon injection inside the cavity. At variance with usual treatments, where the mean-field approximation is used to eliminate the z dependence of the field, our model keeps this dependence, thus allowing for the formation of 3D confined optical structures. We have shown that the simultaneous presence of longitudinal and transverse modes leads to the appearance of spatiotemporal pulses, which is confirmed by numerical simulations and is in agreement with the experimental results.

ACKNOWLEDGEMENTS

U. Bortolozzo acknowledges the support of the EU Contract N. MEIF-CT-2006-041594. A. Montina acknowledges the support of the *Ente Cassa di Risparmio di Firenze*, under the project "dinamiche cerebrali caotiche"

REFERENCES

1. A. E. Siegman, *Lasers*, Oxford University Press (1986).
2. J.L. Bougrenet de la Tocnaye, P. Pellat-Finet and J.P. Huignard, *J. Opt. Soc. Am. B* 3(2), 315-320, (1986).
3. F.T. Arecchi, G. Giacomelli, P.L. Ramazza and S. Residori, *Phys. Rev. Lett.* 65,2531-2534 (1990).
4. U. Bortolozzo, A. Montina, F.T. Arecchi, J.P. Huignard and S. Residori, *Phys. Rev. Lett.* 99,023901-4, (2007).
5. Y. Silberberg, *Opt. Lett.*, 15(22), 1282-1284 (1990).
6. M. Tlidi and P. Mandel, *Phys. Rev. Lett.* 83, 4995-4998 (1999).
7. M. Brambilla, L. Columbo and T. Maggipinto, *J. Opt. B: Quantum Semiclass. Opt.* 6, 197-204 (2004).
8. S.A. Ponomarenko, and G.P. Agrawal, *Opt. Comm.* 261, 1-4 (2006).
9. G. D'Alessandro, *Phys. Rev. A* 46,2791-2802 (1992).
10. B. M. Jost, B. E. A. Saleh, *Phys. Rev. A* 51,1539-1548 (1995).
11. I.C. Khoo, *Liquid Crystals: Physical Properties and Nonlinear Optical Phenomena* (second edition Wiley Interscience, New York, 2007).
12. P. Gunter and J.P. Huignard, *Photorefractive Materials and Their Applications I*, (Springer Science, New York, 2006).
13. U. Bortolozzo, S. Residori, A. Petrosyan, J.P. Huignard, *Opt. Comm.* 263(2), 317-321 (2006).
14. A. Yariv, *Optical Waves in Crystals*, (John Wiley & Sons, New Jersey, 2003)
15. U. Bortolozzo, S. Residori and J.P. Huignard, *Opt. Lett.* 31(14) 2166-2168 (2006).
16. A. Montina, U. Bortolozzo, S. Residori, J.P. Huignard, F.T. Arecchi, "Complex dynamics of a novel optical oscillator based on a liquid crystal light-valve", submitted to *Phys. Rev. A* (2007)